# Electrodisintegration of polarized deuterons

Yu. P. Mel'nik and A. V. Shebeko
*Kharkov Institute of Physics and Technology, 310108 Kharkov, Ukraine*
(Received 5 October 1992)

Dependences of the azimuthal and target asymmetries in the breakup of polarized deuterons by unpolarized electrons on the choice of the deuteron electromagnetic (EM) current model and final-state interaction (FSI) effects are investigated. Possibilities for separation of the structure functions which determine these observables are discussed. Results of the calculations are compared with available data. It has been shown that FSI plays an important role in formation of the asymmetries. In the quasifree region some of them depend considerably on the neutron electric form factor and on the spin-orbit EM interaction with nucleon. The tensor target asymmetries $T_{20}$ and $T_{22}$ calculated for $^2\vec{\mathrm{H}}(e,pn)e'$ under kinematic conditions of the experiment with the electron storage ring VEPP–3 in Novosibirsk have been found to be very sensitive to the meson exchange current contributions.

PACS number(s): 25.30.Fj, 13.40.Fn, 21.45.+v

## I. INTRODUCTION

At present, during the construction of high-duty factor electron accelerators, polarization phenomena in electromagnetic (EM) interactions with atomic nuclei attract a constantly increasing interest [1–3]. In this context the employment of polarized nuclear targets (for example, the deuterium one) opens new possibilities in studying the reaction mechanisms and nuclear properties. The target asymmetries in electrodisintegration of polarized deuterons contain much richer information on the two-body dynamics than in the case with unpolarized particles. These polarization observables depend on the structure functions (SF) which do not occur in the $^2\mathrm{H}(e,e'p)n$ cross sections.

The asymmetries in the $^2\vec{\mathrm{H}}(e,e'p)n$ reaction with tensor polarized deuterons can bring additional information on the deuteron structure, in particular, at small distances. In fact, the corresponding SF calculated within the impulse approximation (IA) are determined by interference of the $S$ and $D$ waves of the deuteron wave function (WF). This observation was an important motivation for extracting the high-momenta components of the WF from the data on the cross sections of the $^2\vec{\mathrm{H}}(e,pn)e'$ reaction at photon point [4].

Of course, the simple IA predictions are needed to be corrected due to various distortion factors, e.g., the final-state interaction (FSI) effects in the $n$-$p$ system. In addition, at large energy and momentum transfers one has to take into account the contributions of non-nucleonic degrees of freedom, viz., meson exchange currents (MEC), isobar configurations (IC) in the deuteron, etc. [5].

Lately [6–9], we have studied the combined influence of FSI and MEC on the formation of angular distributions and polarizations of protons in the $^2\mathrm{H}(e,e'\vec{p})n$ and $^2\mathrm{H}(\vec{e},e'\vec{p})n$ reactions with unpolarized and longitudinally polarized electrons, respectively. The aim of this paper is to extend these investigations for the case with vector- and tensor-polarized deuterons.

As previously, our attention is focused upon kinematic conditions in which the target asymmetries are expressed through the minimal number of SF. According to Ref. [6], the situation most favorable in this respect corresponds to the so-called parallel kinematics when the momenta of outgoing proton and virtual photon are collinear.

At first the tensor asymmetries in the deuteron electrodisintegration were measured in the experiment at Novosibirsk [4] using the electron storage ring VEPP-2 with the electron energy $E = 180$ MeV and the internal target (the polarized deuterium jet). Recently these investigations have been continued with electron storage ring VEPP-3 ($E = 2$ GeV) [10]. Note that the asymmetries in the $^2\vec{\mathrm{H}}(\vec{e},e'p)n$ reaction with vector-polarized deuterons and longitudinally polarized electrons are proposed to be measured at CEBAF [11].

The papers [12,13] were devoted to theoretical descriptions of electrodisintegration of polarized deuterons. In Ref. [13] the tensor asymmetries for the process were calculated within the so-called relativistic IA both in the quasifree peak (QFP) region and, far from this region, under kinematic conditions [4]. A more complete treatment of polarization observables for $^2\vec{\mathrm{H}}(e,e'p)n$ reaction was performed in Ref. [12] taking into account the effects of FSI, MEC, and IC.

Here our consideration of polarization phenomena in electrodisintegration of polarized deuterons is based on the approach developed in Refs. [6,7].

The structure of this paper is the following. In Sec. II the basic formulas for deuteron disintegration with unpolarized electrons and polarized deuterons are given. The target and azimuthal asymmetries, involved in the $^2\vec{\mathrm{H}}(e,e'p)n$ cross sections, are defined in Sec. III and a possibility of the SF separation is discussed. Polarization observables measured in experiment [10] are considered in Sec. IV. Results of our calculations are presented in Sec. V. Finally, Sec. VI contains conclusive remarks.

## II. BASIC FORMULAS

In the one-photon exchange approximation $^2\vec{\mathrm{H}}(e,e'p)n$ cross sections with polarized deuterons in the laboratory

 

frame can be written as

$$\sigma \equiv d^3\sigma/dE'd\Omega_e d\Omega_p = (2\alpha E'/Q^2)^2 l^{\mu\nu} W_{\mu\nu} R, \quad (1)$$

where $\alpha$ is the fine-structure constant, $l_{\mu\nu} = (k'_\mu k_\nu + k'_\nu k_\mu - kk' g_{\mu\nu})/2EE'$ is the leptonic tensor, $g_{\mu\nu}$ is the metric tensor, $k = (E, \mathbf{k})$ and $k' = (E', \mathbf{k}')$ are the 4-momenta of the incident and scattered electrons, respectively, $Q^2 = \mathbf{q}^2 - \omega^2$, $\mathbf{q} = \mathbf{k} - \mathbf{k}'$ ($\omega = E - E'$) is the momentum (energy) transfer, and $R$ is the recoil factor (see, e.g., Ref. [6]). The hadronic tensor $W_{\mu\nu}$ in Eq. (1) is defined by

$$W_{\mu\nu} = \sum_{S,M_S,M_d,M'_d} F_{SM_S\mu M'_d} \rho_{M'_d M_d} F^*_{SM_S\nu M_d}, \quad (2)$$

where $F_{SM_S\mu M_d}$ denotes the matrix element

$$F_{SM_S\mu M_d} = \langle \Psi^{(-)}_{\mathbf{p}_0 SM_S} | J_\mu(\mathbf{q}) | \Psi_{1M_d} \rangle \quad (3)$$

of the deuteron EM current operator $J_\mu = (J_4, \mathbf{J})$ between the initial $|\Psi_{1M_d}\rangle$ and final $|\Psi^{(-)}_{\mathbf{p}_0 SM_S}\rangle = \frac{1}{\sqrt{2}} \sum_T |\Psi^{(-)}_{\mathbf{p}_0 SM_S T0}\rangle$ states of the $n$-$p$ pair with spin $S$, its projection $M_S$, isospin $T$, and relative momentum $\mathbf{p}_0$.

The deuteron density matrix $\rho_{M'_d M_d}$ can be expressed in terms of orientation parameters $P_{JM}$ that characterize the degrees of vector ($J = 1$) and tensor ($J = 2$) target polarizations (cf. Ref. [12]):

$$\rho_{M'_d M_d} = \sum_{JM} C^{JM}_{M'_d M_d} P^*_{JM}, \quad (4)$$

where

$$C^{JM}_{M'_d M_d} = (-1)^{M'_d+1} \left(1 M_d 1 - M'_d | JM\right) / \sqrt{3},$$

$$P_{00} = 1, \; P^*_{JM} = (-1)^M P_{J-M}.$$

Normally one gets the polarized deuterons occupying the atomic levels with different values of spin projection $M_d$ onto the direction of an external magnetic field $\mathbf{H}$ (the $Z$ axis). Thereat the density matrix is diagonal with respect to the basis formed by the states $|\Psi_{1M_d}\rangle$:

$$\rho_{M'_d M_d} = n_{M_d} \delta_{M'_d M_d}, \quad (5)$$

where $n_{M_d}$ is the occupation probability for the level with a given projection $M_d$ onto the chosen quantization axis, $n_{+1} + n_{-1} + n_0 = 1$. In the case only two parameters in the decomposition (4) are independent

$$P_1 \equiv P_{10} = \sqrt{\frac{3}{2}}(n_1 - n_{-1}), \quad (6a)$$

$$P_2 \equiv P_{20} = \frac{1}{\sqrt{2}}(1 - 3n_0). \quad (6b)$$

If the vector $\mathbf{H}$ has an arbitrary orientation with the angles $\theta_H$ and $\phi_H$, then eight parameters in Eq. (4) are connected with $P_1$ and $P_2$ by

$$P_{JM} = P_J e^{iM\phi_H} d^J_{M0}(\theta_H), \quad (7)$$

where $d^J_{M0}(\theta)$ is the Wigner function.

Let us consider the noncoplanar geometry (Fig. 1) when the momentum $\mathbf{q}$ of virtual photon is directed along the $Z$ axis ($\hat{\mathbf{n}}_Z = \mathbf{q}/q$), and the electron scattering plane is coincident with the $X$-$Z$ plane ($\hat{\mathbf{n}}_Y = \mathbf{k} \times \mathbf{k}' / |\mathbf{k} \times \mathbf{k}'|$). The angle between the $X$-$Z$ plane and the plane formed by the momenta $\mathbf{q}$ and $\mathbf{k}_p$ is denoted by $\phi$.

Inserting Eqs. (4) and (7) into Eq. (2) and separating the dependences of the amplitudes (3) on the azimuthal angle $\phi$, we get

$$W_{\mu\nu} = \sum_{JM} e^{iM(\phi - \phi_H)} P_J w^{JM}_{\mu\nu} d^J_{M0}(\theta_H), \quad (8)$$

$$w^{JM}_{\mu\nu} = \sum_{M'_d, M_d} C^{JM}_{M'_d M_d} \sum_{SM_S} f^*_{SM_S\mu M'_d} f_{SM_S\nu M_d}, \quad (9)$$

where $f_{SM_S\mu M_d}$ are the amplitudes (3) at $\phi = 0$, i.e., for the coplanar geometry.

Note the relationships

$$w^{JM}_{\mu\nu} = (-1)^M \left(w^{J-M}_{\nu\mu}\right)^*, \quad (10)$$

$$w^{JM}_{\mu\nu} = (-1)^{J+\delta_{\mu Y}+\delta_{\nu Y}} \left(w^{JM}_{\nu\mu}\right)^*, \quad (11)$$

where the indices $\mu$ and $\nu$ take on the values 4 ($X$,$Y$) for the time (space) components of the hadronic tensor.

When deriving Eq. (11) we employed the symmetry properties

$$f_{S-M_S\mu-M_d} = (-1)^{S+1-M_S-M_d+\delta_{\mu Y}} f_{SM_S\mu M_d}. \quad (12)$$

Furthermore, using Eqs. (8)–(12), one finds

$$\sigma = K \sum_J \sigma^{(J)}, \quad (13)$$

where $K = \sigma_{\rm Mott} R$, $\sigma_{\rm Mott}$ is the Mott cross section.

The separate terms in Eq. (13) determine the contributions due to the disintegration of unpolarized ($J = 0$), vector ($J = 1$), and tensor ($J = 2$) polarized deuterons:

$$\sigma^{(0)} = S^{00}, \quad (14)$$

$$\sigma^{(1)} = P_1 \sum_{M \geq 0} \{S^{1M} \sin[M(\phi - \phi_H)] + \bar{S}^{1M} \cos[M(\phi - \phi_H)]\} d^1_{M0}(\theta_H), \quad (15)$$

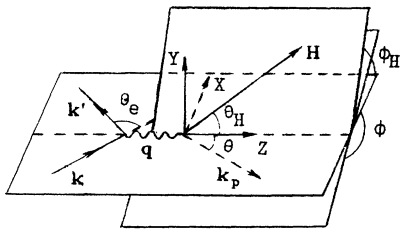


FIG. 1. Geometry for exclusive electron-deuteron scattering with a polarized deuteron target.

$$\sigma^{(2)} = P_2 \sum_{M\geq 0} \{S^{2M}\cos[M(\phi-\phi_H)] + \bar{S}^{2M}\sin[M(\phi-\phi_H)]\} d^2_{M0}(\theta_H). \quad (16)$$

The quantities $S^{JM}$ and $\bar{S}^{JM}$ can be expressed in terms of the $W_i^{JM}$ $(i = L, LT, T, TT)$ and $\bar{W}_i^{JM}$ $(i = LT, TT)$:

$$S^{JM} = \xi^2 W_L^{JM} + \left(\frac{1}{2}\xi + \eta\right) W_T^{JM} + \frac{1}{2}\xi\, W_{TT}^{JM}\cos 2\phi + \xi\sqrt{\xi+\eta} W_{LT}^{JM}\cos\phi, \quad (17)$$

$$\bar{S}^{JM} = \frac{1}{2}\xi\, \bar{W}_{TT}^{JM}\sin 2\phi + \xi\sqrt{\xi+\eta}\, \bar{W}_{LT}^{JM}\sin\phi, \quad (18)$$

$$\xi = Q^2/\mathbf{q}^2, \quad \eta = \tan^2\theta_e/2,$$

where $\theta_e$ is the electron scattering angle. Clearly, the functions $\bar{S}^{JM} = 0$ for the coplanar geometry when the momentum $\mathbf{k}_p$ lies in the $X$-$Z$ plane. The SF $W_i$ $(\bar{W}_i)$ depend on the different current components, viz., the Coulomb SF

$$W_L^{JM} = W_{44}^{JM}, \quad (19)$$

while for the remaining SF one has

$$W_T^{JM} = W_{XX}^{JM} + W_{YY}^{JM}, \quad W_{TT}^{JM} = W_{XX}^{JM} - W_{YY}^{JM},$$

$$\bar{W}_{TT}^{JM} = \bar{W}_{XY}^{JM}, \quad (20)$$

$$W_{LT}^{JM} = -2W_{X4}^{JM}, \qquad \bar{W}_{LT}^{JM} = -W_{Y4}^{JM}. \quad (21)$$

In other words, the SF $W_{LT}$ $(\bar{W}_{LT})$ are determined by the interference of the longitudinal and transverse current components.

We introduced the following notations:

$$W_{\mu\nu}^{JM} = b_{JM}\mathrm{Re}\left(i^J w_{\mu\nu}^{JM}\right), \quad (22)$$

$$\bar{W}_{\mu\nu}^{JM} = \bar{b}_{JM}\mathrm{Im}\left(i^J w_{\mu\nu}^{JM}\right), \quad (23)$$

where $b_{JM} = (1-2\delta_{J2})[2-\delta_{M0}(1+\delta_{J1})]$, $\bar{b}_{JM} = -2[2-\delta_{M0}(1+\delta_{J2})]$.

So, the cross section of electrodisintegration of polarized deuterons contains 24 additional SF together with four SF $W_i^{00}$ $(i = L, LT, T, TT)$ for unpolarized deuterons. Eight of them $W_i^{11}$ $(i = L, LT, T, TT)$ and $\bar{W}_i^{1M}$ $(i = LT, TT)$ are associated with the deuteron vector polarization while the rest $W_i^{2M}$ $(i = L, LT, T, TT)$ and $\bar{W}_i^{21}$, $\bar{W}_k^{22}$ $(i, k = LT, TT)$ appear for tensor polarized deuterons.

Decomposing the final state $\langle\Psi^{(-)}_{\mathbf{p}_0 SM_S}|$ as

$$\langle\Psi^{(-)}_{\mathbf{p}_0 SM_S}| = \langle\Psi^{(1)}_{\mathbf{p}_0 SM_S}| + i\langle\Psi^{(2)}_{\mathbf{p}_0 SM_S}|, \quad (24)$$

where $\langle\Psi^{(2)}_{\mathbf{p}_0 SM_S}| = 0$ in the case with no FSI included, one can write [cf. Eqs. (15)–(16) in Ref. [7]]

$$W_{\mu\nu}^{11} = b_{11}\sum_{M_d', M_d} C^{11}_{M_d' M_d} \sum_{SM_S}\left(f^{(2)*}_{SM_S\mu M_d'} f^{(1)}_{SM_S\nu M_d} - f^{(1)*}_{SM_S\mu M_d'} f^{(2)}_{SM_S\nu M_d}\right), \quad (25)$$

where $f^{(k)}_{SM_S\mu M_d} = \langle\Psi^{(k)}_{\mathbf{p}_0 SM_S}|J_\mu(\mathbf{q})|\Psi_{1M_d}\rangle$ $(k = 1, 2)$. Like this for the $W_{\mu\nu}^{JM}$ with $J = 0, 2$ one gets

$$W_{\mu\nu}^{JM} = i^J b_{JM}\sum_{k=1,2}\sum_{M_d', M_d} C^{JM}_{M_d' M_d}\sum_{SM_S} f^{(k)*}_{SM_S\mu M_d'} f^{(k)}_{SM_S\nu M_d}. \quad (26)$$

It follows from Eq. (25) that $W_i^{11} = 0$ $(i = L, LT, T, TT)$ if one neglects the FSI in the $n$-$p$ pair. The same property has the polarization tensor that determines the proton polarization in the $^2\mathrm{H}(e, e'\vec{p})n$ reaction with unpolarized deuterons (cf. Ref. [7]).

At the same time even without the FSI inclusion polarization properties of the target can be transferred to those observables which are determined by the SF with $J = 0, 2$.

## III. THE SF SEPARATION: TARGET ASYMMETRIES

Contributions of the SF involved can be separated by measuring the vector $A_v$ and tensor $A_t$ target asymmetries. They are defined as

$$A_v = \sigma^{(1)}/P_1\sigma^{(0)}, \quad (27a)$$

$$A_t = \sigma^{(2)}/P_2\sigma^{(0)}. \quad (27b)$$

In these terms one has instead Eq. (13)

$$\sigma(\mathbf{H}) = K\sigma^{(0)}[1 + P_1 A_v + P_2 A_t]. \quad (28)$$

Reversing the direction of the field $\mathbf{H}$ one finds

$$\sigma^{(1)}(-\mathbf{H}) = -\sigma^{(1)}(\mathbf{H}), \quad (29a)$$

$$\sigma^{(2)}(-\mathbf{H}) = \sigma^{(2)}(\mathbf{H}), \quad (29b)$$

so

$$A_v(\theta_H, \phi_H) = [\sigma(\mathbf{H}) - \sigma(-\mathbf{H})]/2P_1 K\sigma^{(0)}, \quad (30a)$$

$$A_t(\theta_H, \phi_H) = [\sigma(\mathbf{H}) + \sigma(-\mathbf{H}) - 2K\sigma^{(0)}]/2P_2 K\sigma^{(0)}. \quad (30b)$$

In the coplanar case $(\phi = 0, \pi)$ the vector asymmetry $A_v$ vanishes if the vector $\mathbf{H}$ lies in the reaction plane. At a certain value of the proton emission angle $\theta$ [14] the quantity $A_v$ takes on a maximum value when the field is

normal to the plane, i.e., $\theta_H = \phi_H = \frac{\pi}{2}$,

$$A_v^{11} = \pm\frac{1}{\sqrt{2}} S^{11}/S^{00}, \tag{31}$$

where the upper (lower) sign is used for $\phi = 0$ ($\pi$).

In addition, let us consider the situation with $\mathbf{k}_p \| \mathbf{q}$, i.e., at $\theta = 0$ or $\pi$, then only one of four $W_i^{11}$ ($i = L, LT, T, TT$) survives (cf. Ref. [6]):

$$A_v^{11} = \frac{1}{\sqrt{2}} \frac{\xi\sqrt{\xi+\eta} W_{LT}^{11}}{\xi^2 W_L + \left(\frac{1}{2}\xi + \eta\right) W_T}. \tag{32}$$

For brevity the SF $W_i^{00}$ ($i = L, LT, T, TT$) are henceforth denoted by $W_i$. Note the relationships between them and the corresponding SF $W_i$ ($i = C, I, T, S$) defined in [6,7] for the case in question: $W_C = W_L$, $W_I = (1 - 2\delta_{\phi\pi}) W_{LT}$, $W_S = W_{TT}$, and $W_T = W_T^{00} - W_{TT}$.

Therefore, the interference SF $W_{LT}^{11}$ could be extracted by analyzing the vector asymmetry $A_v^{11}$ [cf. Refs. [6,7] where one has demonstrated that the outgoing proton polarization in $^2\mathrm{H}(e, e'\vec{p})n$ for parallel kinematics is determined by a single SF $\Sigma_I$].

The angular dependence $W_{LT}^{11}(\theta)$ can be explored on measuring the azimuthal asymmetries

$$Z_\pm^{11} = \frac{\sigma^{(1)}(\phi=0) + \sigma^{(1)}(\phi=\pi)}{P_1[\sigma^{(0)}(\phi=0) \pm \sigma^{(0)}(\phi=\pi)]} = \frac{\sigma(\phi=0,\mathbf{H}) - \sigma(\phi=0,-\mathbf{H}) + \sigma(\phi=\pi,\mathbf{H}) - \sigma(\phi=\pi,-\mathbf{H})}{2P_1 K[\sigma^{(0)}(\phi=0) \pm \sigma^{(0)}(\phi=\pi)]}. \tag{33a}$$

In fact, one has

$$Z_+^{11} = \frac{1}{\sqrt{2}} \frac{\xi\sqrt{\xi+\eta} W_{LT}^{11}}{\xi^2 W_L + \left(\frac{1}{2}\xi + \eta\right) W_T + \frac{1}{2}\xi W_{TT}} \tag{33b}$$

and

$$Z_-^{11} = \frac{1}{\sqrt{2}} W_{LT}^{11}/W_{LT}. \tag{33c}$$

Note that

$$Z_+^{11}/Z_-^{11} = \Sigma_\phi = [\sigma^{(0)}(\phi=0) - \sigma^{(0)}(\phi=\pi)]/[\sigma^{(0)}(\phi=0) + \sigma^{(0)}(\phi=\pi)],$$

where $\Sigma_\phi$ is the azimuthal asymmetry of the $^2\mathrm{H}(e, e'\vec{p})n$ cross sections with unpolarized particles.

Resorting to the SF separation for tensor-polarized deuterons one can see that the component $A_t^{20}$ of $A_t = \sum\limits_{M\geq 0} A_t^{2M}$ is equal to

$$A_t^{20} = A_t(0,0) = S^{20}/S^{00}. \tag{34}$$

This expression is simplified in parallel kinematics

$$A_t^{20} = \frac{\xi^2 W_L^{20} + \left(\frac{1}{2}\xi + \eta\right) W_T^{20}}{\xi^2 W_L + \left(\frac{1}{2}\xi + \eta\right) W_T}. \tag{35}$$

Again, introducing azimuthal asymmetries

$$Z_\pm^{20} = \frac{\sigma^{(2)}(\phi=0) - \sigma^{(2)}(\phi=\pi)}{P_2[\sigma^{(0)}(\phi=0) \pm \sigma^{(0)}(\phi=\pi)]} \tag{36}$$

one gets

$$Z_+^{20} = \frac{\xi\sqrt{\xi+\eta} W_{LT}^{20}}{\xi^2 W_L + \left(\frac{1}{2}\xi + \eta\right) W_T + \frac{1}{2}\xi W_{TT}}, \tag{37a}$$

$$Z_-^{20} = W_{LT}^{20}/W_{LT}, \tag{37b}$$

i.e., these polarization observables are connected in a simple way with the SF $W_{LT}^{20}$.

Other tensor asymmetries can be determined by changing the direction of $\mathbf{H}$

$$A_t^{21} = A_t(0,0) - 4A_t\left(\frac{\pi}{4}, \frac{\pi}{4}\right), \tag{38}$$

$$A_t^{22} = A_t(0,0) + 2A_t\left(\frac{\pi}{2}, \frac{\pi}{2}\right) \tag{39}$$

or using Eqs. (14) and (16) one can write

$$A_t^{2M} = \beta_M S^{2M} \cos M\phi \,/S^{00}, \quad \beta_M = (-1)^{M+1}\sqrt{3/M} \tag{40}$$

$$(M = 1, 2; \quad \phi = 0, \pi).$$

Similarly, Eqs. (32) and (35) in parallel kinematics yield

$$A_t^{21} = \sqrt{3} \frac{\xi\sqrt{\xi+\eta} W_{LT}^{21}}{\xi^2 W_L + \left(\frac{1}{2}\xi + \eta\right) W_T}, \tag{41}$$

$$A_t^{22} = -\sqrt{\frac{3}{8}} \frac{\xi W_{TT}^{22}}{\xi^2 W_L + \left(\frac{1}{2}\xi + \eta\right) W_T}. \tag{42}$$

Of great interest also are the azimuthal asymmetries

$$Z_+^{2M} = \beta_M \frac{\xi\sqrt{\xi+\eta}W_{LT}^{2M}}{\xi^2 W_L + \left(\frac{1}{2}\xi+\eta\right)W_T + \frac{1}{2}\xi W_{TT}}, \quad (43a)$$

$$Z_-^{2M} = \beta_M W_{LT}^{2M}/W_{LT} \quad (M=1,2). \quad (43b)$$

Each of them is proportional to the SF $W_{LT}^{2M}$.

Again note that $Z_+^{2M}/Z_-^{2M} = \Sigma_\phi$.

## IV. ELECTRODISINTEGRATION OF POLARIZED DEUTERONS AT PHOTON POINT ($Q^2 = 0$). EXPERIMENTS IN NOVOSIBIRSK

In the experiment [10] in question the scattered electron was not detected, but the proton and the neutron were registered in coincidence. From various $p$-$n$ coincidence the events that were selected corresponded to the inelastic $e$-$d$ scattering at small angles, i.e., the situation with $\theta_e \approx 0°$. Therefore, under these kinematic conditions the virtual photon absorbed by the deuteron differs only slightly from the real one ($Q^2 \approx 0$, $q = \omega$).

During the measurements the average degree $P_{ZZ}$ of the tensor polarization of a gas jet was equal to $P_{ZZ} = \pm(0.778\pm0.075)$. Note that $P_2 = P_{ZZ}/\sqrt{2}$.

In the case of interest we find

$$\sigma^{(0)} = W_T,$$

$$\sigma^{(1)} = P_1 W_T^{11} \sin(\phi - \phi_H) d_{10}^1(\theta_H), \quad (44)$$

$$\sigma^{(2)} = P_2 \sum_{M\geq 0} W_T^{2M} \cos[M(\phi-\phi_H)] d_{M0}^2(\theta_H).$$

The experimental arrangement was chosen as [15]

$$\theta_{H_1} = \theta_{H_2} = 90°,$$

$$\phi_{H_1} = 135°, \quad \phi_{H_2} = 45°, \quad \phi_1 = 225°, \quad \phi_2 = 315° \quad (45)$$

with the proton emission angle in the final $n$-$p$ center of mass system (the c.m. frame) $\theta^* = 88°$. This value and the values $\phi_1$ and $\phi_2$ of proton azimuthal angle determine positions of two proton detectors in the plane normal to the electron beam direction. The quantities extracted from the measurement are given by

$$a_{20} = \frac{\sum\limits_{i,j=1,2}(N_{j+}^i - N_{j-}^i)}{\sum\limits_{i,j=1,2}(N_{j+}^i + N_{j-}^i)}, \quad (46)$$

$$a_{22} = \frac{\sum\limits_{i,j=1,2}(-1)^{\delta_{ij}}(N_{j-}^i - N_{j+}^i)}{\sum\limits_{i,j=1,2}(N_{j+}^i + N_{j-}^i)}, \quad (47)$$

where in the counting rate $N_{j\pm}^i$ the upper index labels the detection system and the lower one coincides with the field index in $\mathbf{H}_j$, and the sign index is the sign of $P_{ZZ}$.

In our notations

$$a_{20} = -\frac{1}{\sqrt{8}}|P_{ZZ}|T_{20}, \quad (48)$$

$$a_{22} = -\frac{\sqrt{3}}{4}|P_{ZZ}|T_{22}, \quad (49)$$

$$T_{JM} = W_T^{JM}/W_T.$$

It is proved that in the plane wave IA (PWIA)

$$T_{20} = 2u(k_n)d_{00}^2(\theta_n), \quad T_{22} = 4u(k_n)d_{20}^2(\theta_n), \quad (50)$$

$$u(k_n) = u_2(k_n)\left[u_0(k_n) - \frac{1}{\sqrt{8}}u_2(k_n)\right] \Big/ [u_0^2(k_n) + u_2^2(k_n)], \quad (51)$$

where $u_0(k_n)$ [$u_2(k_n)$] is the $S$ ($D$) component of the deuteron WF, and $k_n$ ($\theta_n$) is the neutron momentum (emission angle) in the laboratory system with the $Z$ axis along the vector $\mathbf{q}$.

To derive the SF $W_T^{21}$ the counting rates $N_{j\pm}^i$ could be measured for two configurations

$$\theta_{H_1} = 45°, \quad \phi_{H_1} = 135° \quad (52a)$$

and

$$\theta_{H_2} = 135°, \quad \phi_{H_2} = 45° \quad (52b)$$

retaining the values of $\theta^*$, $\phi_1$, $\phi_2$, and forming the ratio

$$a_{21} = \frac{\sum\limits_{i,j=1,2}\left((-1)^{\delta_{i2}}N_{j+}^i + (-1)^{\delta_{i1}}N_{j-}^i\right)}{\sum\limits_{i,j=1,2}(N_{j+}^i + N_{j-}^i)}. \quad (53)$$

Indeed, in this case

$$a_{21} = -\frac{\sqrt{3}}{8}|P_{ZZ}|T_{21}. \quad (54)$$

Let us write the corresponding PWIA expression

$$T_{21} = -4u(k_n)d_{10}^2(\theta_n). \quad (55)$$

Finally, the combination

$$a_{11} = -\frac{\sum\limits_{i=1,2}(-1)^{\delta_{i1}}(N_{i+}^i + N_{i-}^i)}{\sum\limits_{i,j=1,2}(N_{j+}^i + N_{j-}^i)} \quad (56)$$

yields the vector asymmetry

$$a_{11} = -\frac{1}{\sqrt{2}}P_1 T_{11} \quad (57)$$

for the arrangement (45).

## V. RESULTS AND DISCUSSION

Details of our calculations of the reaction amplitudes can be found in [7]. The calculations were performed with the Paris potential [16]. The FSI distortions were taken into account in the partial $p$-$n$ scattering states with the total angular momentum $J \leq J_{\max} = 2$ in the QFP region (the MIT kinematics) and $J \leq J_{\max} = 3$ far from the region (the Novosibirsk kinematics). Note that the results of our calculations have a good convergence with respect to the FSI inclusion in higher partial waves. For example, the angular dependences of the asymmetries undergo small changes as $J_{\max}$ increases, viz., the corresponding variations do not exceed a few percent.

The MEC included are due to one-pion exchange with the $\pi NN$ vertices modified by the nucleon finite-size effects. The corresponding phenomenological $\pi NN$ form factors (FF) in the monopole form depend on a cutoff parameter $\Lambda$. Two models, with $G_E^n = 0$ and $G_E^n = \tau \kappa_n G_E^p$ [17], where $\tau = -Q^2/4M^2$ ($M$ is the nucleon mass), $\kappa_n$ is the neutron anomalous magnetic moment, were chosen for the neutron electric FF $G_E^n$.

As in Ref. [7], we distinguish the direct mechanism of the proton knockout (PWIA) and the recoil mechanism due to the EM interaction with the neutron-spectator [the plane wave Born approximation (PWBA)]. Respectively, our calculations with the distorted waves are marked by the DWIA and DWBA.

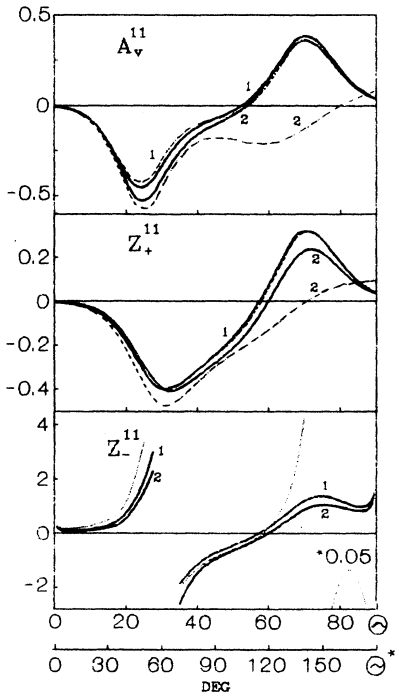


FIG. 2. Angular dependences of the vector asymmetries for $^2\vec{\mathrm{H}}(e,e'p)n$. Calculations were made in the DWBA and DWIA (dashed curves 1 and 2, respectively), in the MEC model (see, e.g., [21]) for the cutoff parameter $\Lambda = 4m_\pi$, where $m_\pi$ is the pion mass, with (solid) and without (dotted) addition of the SO interaction to the hadronic current. All curves correspond to the case with $G_E^n$ of Ref. [17], except solid curves 2 calculated with $G_E^n = 0$.

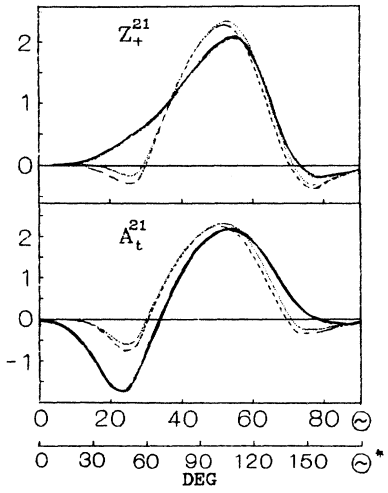


FIG. 3. The asymmetries $A_t^{21}$ and $Z_+^{21}$ with (solid curve) and without (dashed and dotted curves) the deuteron $D$ wave. The latter is calculated in the DWBA, the rest — with inclusion of FSI and MEC [21].

The results shown in Figs. 2–6 [18] were obtained at the values of $E = 880$ MeV, $E' = 738$ MeV, and $\theta_e = 37°$, i.e., for quasifree kinematics, as the Bjorken variable $x = Q^2/2M\omega = 1$. A number of useful kinematic rela-

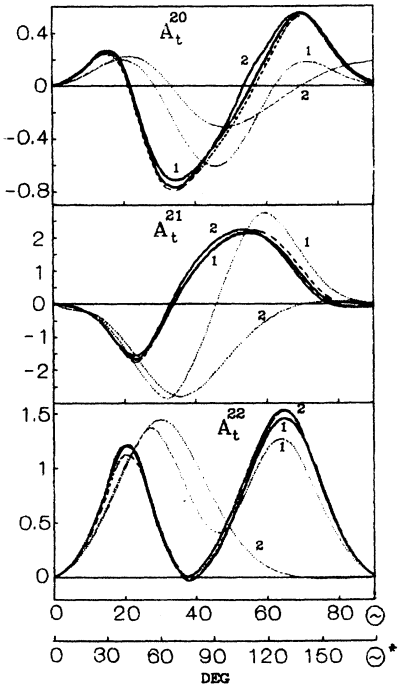


FIG. 4. Angular dependences of the tensor asymmetries $A_t^{2M}$ for $^2\vec{\mathrm{H}}(e,e'p)n$. The curves were calculated in the PWBA (PWIA) — dotted 1 (2), in the DWBA — dashed. Other differences between curves are the same as in Fig. 2.

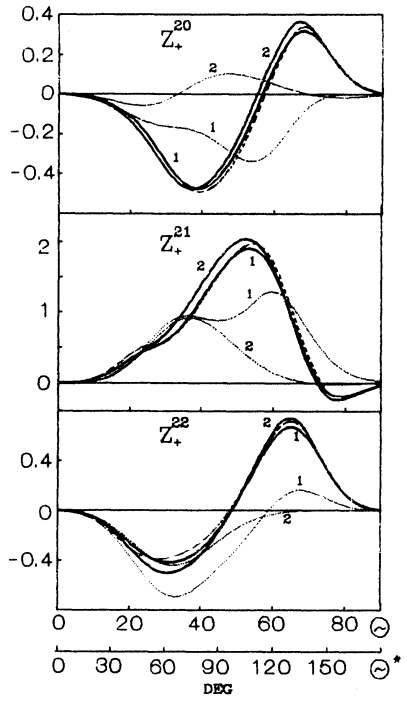


FIG. 5. Same as in Fig. 4 for the asymmetries $Z_+^{2M}$.

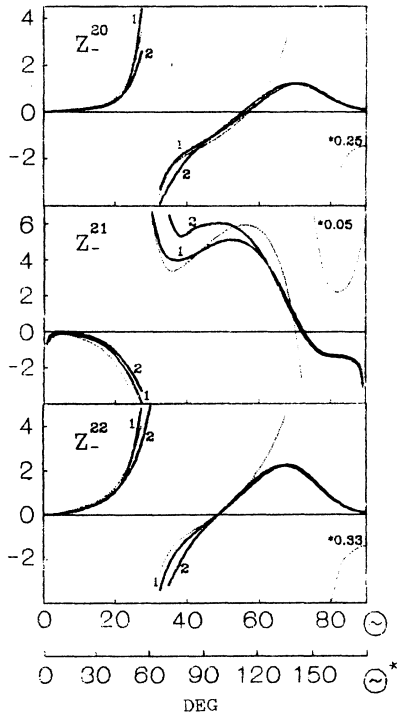


FIG. 6. Same as in Fig. 5 for the asymmetries $Z_-^{2M}$.

tionships for the case can be found in Appendix A. Note that this choice of kinematic parameters corresponds to conditions of the MIT I experiment [20]. Under these conditions the values of the proton emission angle do not exceed the limiting value $\theta_{\rm lim} = 90°$ (parallel kinematics for the recoil neutron with the momentum $\mathbf{k}_n = \mathbf{q}$). The value $\theta = 0°$ corresponds to parallel kinematics for the outgoing proton.

A detailed analysis shows that the direct reaction mechanism is prevalent in the $e'p$ coincidence cross sections at the values $\theta \leq 45°$. When increasing $\theta$ the EM interaction with neutron becomes more important. In particular, we see that the asymmetries considered can undergo qualitative changes because of a strong interplay between the direct and recoil mechanisms. As mentioned in Sec. III, the asymmetry $A_v$ has some common features with the outgoing proton polarization $P$ in $^2\mathrm{H}(e,e'\vec{p})n$ (in particular, it takes on the zero value with the FSI not included). The vectors $\mathbf{A}_v$ and $\mathbf{P}$ are perpendicular to the reaction plane for the EM current model without violations of $P$ and $T$ invariances (cf. the discussion in Ref. [7]). In addition, in parallel kinematics each of them is expressed through a single interference SF, viz., $W_{LT}^{11}$ ($\Sigma_I$) for $A_v$ ($P$). Moreover, transitions between the same spin states of the $n$-$p$ system contribute $W_{LT}^{11}$ and $\Sigma_I$.

As seen in Fig. 2, the inclusion of the FSI gives the values of $A_v^{11}$ accessible for measurements at intermediate angles $\theta$. The same is valid for the azimuthal asymmetry $Z_+^{11}$.

Relativistic corrections arising from the spin-orbit (SO) EM interaction with the nucleon manifest themselves (sometimes appreciably) in quasifree kinematics. Note that relativistic effects (in particular, due to the Darwin-Foldy and SO terms in the EM current operator) for $^2\mathrm{H}(\vec{e},e'p)n$ reaction in the QFP region have been investigated recently in Ref. [22]. This work extends previous studies [23,24] for the deuteron photodisintegration.

As shown in Fig. 2, the inclusion of the SO interaction leads to essential variations of the $Z_-^{11}$ angular dependence at $\theta > 60°$. These variations are closely connected with the respective changes of the angular dependence of $W_{LT}$. In particular, the SF changes its sign at $\theta \simeq 76°$ as the SO contribution is not included. Like the asymmetry $Z_-^{11}$ the observables $Z_-^{2M}$ are rather sensitive to the contribution as well (see Fig. 6).

For the tensor target asymmetries $A_t^{2M}$ and $Z_\pm^{2M}$ displayed in Figs. 3–6 one should write down the simple relationships in the PWIA

$$A_t^{2M} = Z_-^{2M} = \alpha_{2M} u(k_n) d_{M0}^2(\theta_n), \tag{58}$$

$$Z_+^{2M} = \Sigma_\phi A_t^{2M}, \tag{59}$$

$$\alpha_{20} = 2, \quad \alpha_{2M} = 4(-1)^M \beta_M \quad (M = 1,2).$$

It follows from Eqs. (51), (58), and (59) that the asymmetries vanish identically in the case of a pure $S$ wave deuteron. One can show that this property retains for all the asymmetries (excepting $A_t^{20}$ and $A_t^{22}$) in the PWBA. However, the situation drastically changes after taking into account the FSI when the observables considered assume nonzero values not only owing to an interference of the $S$ and $D$ components of the deuteron WF [cf. Eq. (51)]. In other words, structure properties are

strongly obscured by rescattering effects.

Nevertheless, we see in Fig. 3 essential differences between the quantities calculated with and without inclusion of the $D$ component at the proton emission angle $\theta = 15°$–$30°$ that correspond to the range of recoil momenta $k_n = 140$–$305$ MeV/$c$. Moreover, the quantity $Z_+^{21}$ changes its sign if the $D$ wave is switched off.

We also reveal a noticeable dependence of the vector asymmetries on the choice of the $G_E^n$ model. For example, the quantity $A_v^{11}$ ($Z_+^{11}$) changes its value at $\theta = 25°$ ($70°$) almost by 15% (25%) (Fig. 2). The tensor asymmetries depend on the $G_E^n$ model to lesser extent (see Fig. 4). Note that similar results were obtained in Ref. [12] where the tensor asymmetry $A_t^{20}$ [denoted there as $A_d^T(0,0)$] was calculated with other models for $G_E^n$.

One should emphasize that unlike the authors of Ref. [12], we employ the Dirac FF instead of the Sachs nucleon FF. In addition, polarization observables in [12] were calculated in the c.m. frame while we prefer to present our results in the laboratory frame. General transformation properties of polarization observables for the deuteron electrodisintegration when passing from one to another frame were considered in Appendix C of our paper in Ref. [9]. In this connection we would like to recall that the deuteron density matrix remains unchanged with respect to the boost along the **q** direction.

The relations of the SF (19)–(21) and the target asymmetries (27) to the corresponding quantities considered in Ref. [12] are given in Appendix B.

As seen in Figs. 2, 4, and 5 (cf. the solid curves 1 and dashed ones) these asymmetries have a weak dependence on the two-body reaction mechanisms due to the MEC for quasifree kinematics.

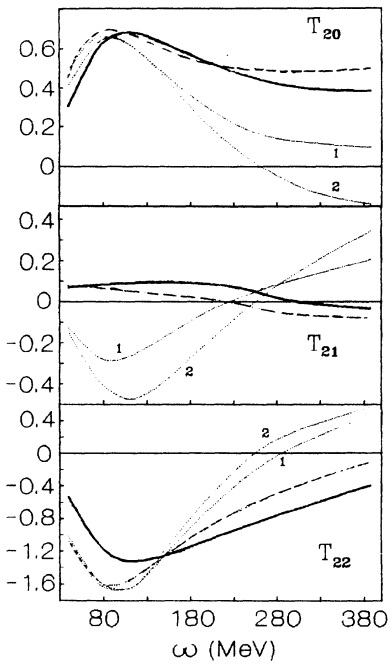


FIG. 7. Tensor asymmetries $T_{2M}$ for $^2\vec{\mathrm{H}}(e,pn)e'$ vs the energy transfer for the VEPP-3 kinematics. The curves were calculated in the PWBA (PWIA) — dotted 1 (2), in the DWBA — dashed, and with taking into account the MEC ($\Lambda = 4m_\pi$) — solid.

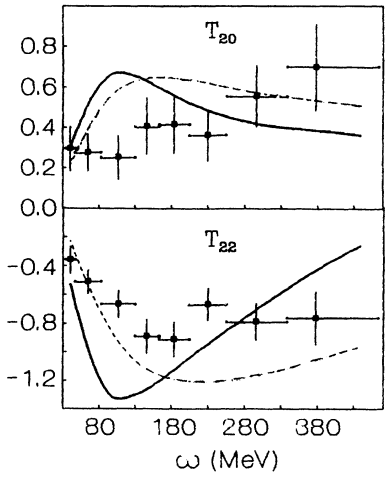


FIG. 8. Comparison of the calculated asymmetries $T_{20}$ and $T_{22}$ with the data [10]. The solid (dashed) curves were calculated including FSI effects in the MEC model with $\Lambda = 4m_\pi$ ($\Lambda = 1.2$ GeV).

We face another situation considering the tensor asymmetries $T_{2M}$ under conditions of the measurements in Novosibirsk [10]. In fact, our results for these quantities in Fig. 7 depend essentially on the MEC contributions. The same is valid for the FSI effects. These findings are typical since we are far from quasifree kinematics in the inelastic $e$-$d$ scattering. It is the case of the experiment [10].

We also see in Fig. 8 a high sensitivity of the calculated asymmetries to the MEC models with hard and soft $\pi NN$ FF. Certainly, the inclusion of such important ingredients as FSI and MEC is necessary for describing the data [10].

Note that the results displayed in Fig. 8 are in agreement with those obtained in Refs. [25,26]. Our preliminary results presented in [10] underestimated the asymmetry $T_{22}$ because of an error in our computer code.

## VI. CONCLUSIVE REMARKS

The main conclusions of the paper can be summarized as follows.

(i) In contrast with the opinion that the FSI effects are expected to be small in quasifree region we have observed a strong dependence of the asymmetries considered on the FSI distortions in the $n$-$p$ scattering states. The exceptions are two situations for proton emission angles close to $\theta = 0°$ and $\theta = 90°$ (parallel kinematics for the proton and the neutron, respectively). So, even in the quasifree region, the FSI effects can make it more complicated to obtain direct information on the deuteron structure (especially, at short distances).

(ii) As to the influence of MEC on these asymmetries it is still rather weak in quasifree region at all $\theta$ values accepted.

(iii) The azimuthal asymmetries $Z_{\pm}^{JM}$, determined longitudinal-transverse interference of the deuteron EM current components, are sensitive to the choice of the neutron electric FF at intermediate $\theta$ values ($0° < \theta < 90°$).

We have seen the most appreciable effect from the variation of $G_E^n$ for the ratio of two interference SF $Z_{-}^{21} = W_{LT}^{21}/W_{LT}$ within the range $30° < \theta < 60°$. Since this effect is observed against a rather weak dependence of $Z_{-}^{21}$ on MEC contributions its measurements can be useful to verify the predictions of modern theories of nuclear structure. Of course, one should keep in mind that the cross sections at these intermediate $\theta$ values are much smaller than for parallel kinematics.

(iv) We have found the kinematic conditions favorable for the SF separation in the $^2\vec{\mathrm{H}}(e,e'p)n$ reaction. In order to fulfill this procedure it is sufficient to carry out some in-plane measurements of the cross sections for the reaction.

(v) The tensor asymmetries $T_{2M}$ for $^2\vec{\mathrm{H}}(e,pn)e'$ calculated under the kinematic conditions of the VEPP-3 experiment, i.e., far from quasifree region, depend considerably on the MEC effects.

To get a reliable information on the deuteron wave function at short distances from such polarization experiments it is necessary to improve an accuracy of the available data. In addition, various reaction mechanisms generated by the exchange of heavier mesons and the $\Delta$-isobar excitation should be included. Of course, other relativistic effects in the deuteron electrodisintegration should be studied as well.

Finally, the results of our calculations have demonstrated that the asymmetries discussed can take on the values accessible for measurements. The latter can be fulfilled at a new qualitative level with installation of high duty-cycle electron accelerators.

We are very grateful to Dr. D. M. Nikolenko and his colleagues from Institute of Nuclear Physics (Novosibirsk) for sending us the recent data before their publication.

## APPENDIX A

Here we consider in more detail the situation with

$$x = Q^2/2M\omega = 1. \tag{A1}$$

Then, assuming $M_p = M_n = M$, one has for the invariant

$$s = (\omega + M_d)^2 - \mathbf{q}^2,$$

$$s = 4M^2\left(1 + \frac{\omega}{2M}\right)\left[1 - \frac{\epsilon_d}{M} + O\left(\frac{\epsilon_d^2}{M^2}\right)\right], \tag{A2}$$

where $M_d$ ($\epsilon_d > 0$) is the deuteron mass (binding energy).

The limiting angle $\theta_{\mathrm{lim}}$ is determined by

$$\sin^2\theta_{\mathrm{lim}} = (\gamma_p^* v_p^*/\gamma v)^2 = s k_p^{*2}/M^2\mathbf{q}^2 \le 1, \tag{A3}$$

where $v$ ($v_p^*$) is the velocity of the c.m. frame [19] relative to the laboratory frame (the knocked-out proton in the c.m. frame), $\gamma$ and $\gamma_p^*$ are the corresponding Lorentz factors.

According to Eq. (A2), we find

$$\sin^2\theta_{\mathrm{lim}} = \left(1 - \frac{\epsilon_d}{M}\right)\left[1 - \frac{2\epsilon_d(1+\omega/2M)}{\omega}\right]. \tag{A4}$$

So, under the condition (A1) $\theta_{\mathrm{lim}} = \frac{\pi}{2}$ to an accuracy of the terms $\sim \epsilon_d/M \ll 1$ and $\epsilon_d/\omega \ll 1$.

Moreover, using the Lorentz transformation

$$\mathbf{k}_p^* = \mathbf{k}_p + [\mathbf{k}_p\mathbf{q}/(\omega + M_d + \sqrt{s}) - E_p]\mathbf{q}/\sqrt{s}, \tag{A5}$$

where $E_p = \sqrt{\mathbf{k}_p^2 + M^2}$ is the proton energy in the laboratory frame, and neglecting the terms $\sim \epsilon_d/M$, $\epsilon_d/\omega$, and $\omega^2/M^2 \ll 1$, one can demonstrate that

$$\cos\theta^* = \cos 2\theta - \frac{\omega}{4M}\sin^2 2\theta, \tag{A6}$$

i.e., $\theta^* = 2\theta$ in a good approximation if the Bjorken variable $x = 1$ and $\omega/4M \ll 1$.

## APPENDIX B

The SF $W_{L,T,LT,TT}^{JM}$ and $\bar{W}_{LT,TT}^{JM}$ calculated in the laboratory system are related to the corresponding SF $f_{L,T,LT,TT}^{JM}$ [12] referred to the c.m. frame [see Eq. (86) in [12]] as

$$W_k^{JM} = d_k f_k^{JM} \ (k = L, T) \tag{B1}$$

and

$$W_k^{JM} = d_k(2 - \delta_{M0})\frac{1}{2}\left[f_k^{JM} + (-1)^{J-M} f_k^{J-M}\right], \tag{B2}$$

$$\bar{W}_k^{JM} = d_k(2-\delta_{M0})(1-2\delta_{J2})\frac{1}{2}\left[f_k^{JM} - (-1)^{J-M} f_k^{J-M}\right] \quad (k = LT, TT). \tag{B3}$$

Here we have used the following notations:

$$d_k = \frac{c\bar{\rho}_k}{\sigma_{\mathrm{Mott}} R}\frac{d\Omega_{np}^*}{d\Omega_p}, \tag{B4}$$

$$\frac{1}{\beta^2}\bar{\rho}_L = \bar{\rho}_T = -\bar{\rho}_{TT} = \frac{\sqrt{2}}{\beta}\bar{\rho}_{LT} = \frac{Q^2}{2\eta}, \tag{B5}$$

where the kinematical factor $c$ is determined in Ref. [12], $\beta = |\mathbf{q}|/|\mathbf{q}^*|$.

The Jacobian in Eq. (B4) transforming the coincidence cross sections from the c.m. frame to the laboratory one is given by

$$\frac{d\Omega_{np}^*}{d\Omega_p} = \frac{k_p}{k_p^*}\frac{1}{\gamma\left[1 - \frac{E_p}{k_p} v\cos\theta\right]}. \tag{B6}$$

In our opinion, the formulas (13)–(16) are more convenient to analyze the polarization observables compared to expressions (79) from Ref. [12] because the former include the SF with $M \geq 0$ only.

As to the target asymmetries (30), they are connected with the asymmetries $A_d^V$ and $A_d^T$ [12] as follows:

$$A_v = A_d^V, \qquad A_t = A_d^T. \tag{B7}$$


[1] W. Meyer, Nucl. Phys. **A446**, 381 (1985).
[2] V. Burkert, Report CEBAF-PR-86-008, 1986.
[3] F. Gross, in *Report of the 1987 Summer Study Group* (CEBAF, Newport News, Virginia, 1988), p. 183.
[4] M.V. Mostovoy, D.M. Nikolenko, K.T. Ospanov, S.G. Popov, I.A. Rachek, Yu.M. Shatunov, D.K. Toporkov, E.P. Tsentalovich, B.B. Wojtzehovsky, V.G. Zelevinsky, G.A. Naumenko, and V.N. Stibunov, Phys. Lett. B **188**, 181 (1987).
[5] H. Arenhövel, Nucl. Phys. **A384**, 287 (1982).
[6] A.Yu. Korchin, Yu.P. Mel'nik, and A.V. Shebeko, Yad. Fiz. **48**, 387 (1988).
[7] A.Yu. Korchin, Yu.P. Mel'nik, and A.V. Shebeko, Few-Body Syst. **9**, 211 (1990).
[8] A.Yu. Korchin, Yu.P. Mel'nik, and A.V. Shebeko, J. Phys. (Paris) Colloq. **51**, C6-499 (1990).
[9] Yu.P. Mel'nik and A.V. Shebeko, Contribution to PANIC XII, Abstracts of Contributed Papers, Boston, 1990, p. I–44; Few-Body Syst. **13**, 59 (1992).
[10] B.B. Wojtzehovsky, S.I. Mishnev, D.M. Nikolenko, S.G. Popov, I.A. Rachek, A.B. Temnykh, D.K. Toporkov, E.P. Tsentalovich, S.L. Belostotsky, V.V. Nelubin, V.V. Sulimov, and V.N. Stibunov, Report INP 92-19, Novosibirsk, 1992.
[11] D. Day, spokesperson, CEBAF Proposal 89-018, 1989 (unpublished).
[12] H. Arenhövel, W. Leidemann, and E.L. Tomusiak, Z. Phys. A **331**, 123 (1988); **334**, 363 (1989).
[13] M.P. Rekalo, G.I. Gakh, and A.P. Rekalo, Vopr. Atom. Nauki i Tekh., Ser.: General and Nuclear Physics (Moscow) **2**(38), 40 (1987).
[14] Henceforth $\theta$ is the angle between the proton momentum $\mathbf{k}_p$ and the transfer momentum $\mathbf{q}$ in the laboratory system.
[15] Other details one can find in Ref. [4].
[16] M. Lacombe, B. Loiseau, J.M. Richard, R. Vinh Mau, J. Côtè, P. Pirès, and R. de Tourreil, Phys. Rev. C **21**, 861 (1980).
[17] A.O. Barut, D. Corringan, and H. Kleinert, Phys. Rev. Lett. **20**, 167 (1968).
[18] All the asymmetries $A_v$ and $A_t$ are shown for in-plane geometry with $\phi = 0$.
[19] Henceforth all quantities in the c.m. frame will be marked with an asterisk.
[20] J.M. Finn, R.W. Lourie, C.F. Perdrisat, and P.E. Ulmer, spokespersons, MIT-Bates Proposal 88-21, 1989 (unpublished).
[21] M.A. Maize and Y.E. Kim, Nucl. Phys. **A420**, 365 (1984).
[22] B. Mosconi and P. Ricci, Nucl. Phys. **A517**, 483 (1990).
[23] A. Cambi, B. Mosconi, and P. Ricci, Phys. Rev. Lett. **48**, 462 (1982); J. Phys. G **10**, L11 (1984).
[24] P. Wilhelm, W. Leidemann, and H. Arenhövel, Few-Body Syst. **3**, 111 (1988).
[25] K.-M. Schmitt and H. Arenhövel, Few-Body Syst. **7**, 95 (1989).
[26] M.I. Levchook, Report IP-609, Minsk, 1990.